Bulletin of Mathematical Biology (2021) 83:37
https://doi.org/10.1007/s11538-021-00866-8

Society for Mathematical Biology

ORIGINAL ARTICLE

Diffusive Interface Model for Actomyosin Driven Cell Oscillations

Xiaoqiang Wang[1] · **Liyong Zhu**[2]

Received: 23 February 2020 / Accepted: 8 February 2021 / Published online: 3 March 2021

Abstract

In this paper, we build phase-field models for the actomyosin driven cell oscillations. In our modeling, an oscillation starts from an actin cortex breakage. After the breakage, due to the unbalanced distribution of actin and myosin, there is unbalanced contraction force in different membrane components, which then results in the lipids transferring to the bulged membrane compartment. As such we can observe a cell oscillation. During the whole process, the actin and myosin polymerization and depolymerization play important roles. We give detailed formulations under the framework of phase-field methodology, in which phase-field functions are used to describe different parts of the cell membrane, integrated with the distribution of the actin and myosin at different components. The whole system is described as a set of time-dependent partial differential equations in three-dimensional space. Forward Euler method is used to solve the system. The spectral method is used for spatial discretizations for efficiency and accuracy purpose. Given carefully selected parameters, three-dimensional simulations are performed and compared with biological images. The simulations prove that actomyosin dynamics are the major reasons for cell oscillations. Further, our method can be easily extended into the simulations of cell polarization. We also compared our numerical simulations with biological experiments. This modeling gives an example of applying diffusive interface methods toward complex biology experiments.

Keywords Cell membrane · Cell oscillation · Actin filaments · Elastic bending energy · Phase-field model · Numerical methods

✉ Xiaoqiang Wang
wwang3@fsu.edu

Liyong Zhu
liyongzhu@buaa.edu.cn

[1] Department of Scientific Computing, Florida State University, Tallahassee, FL 32306-4120, USA

[2] School of Mathematics and Systems Science, Beihang University, Beijing 100191, People's Republic of China

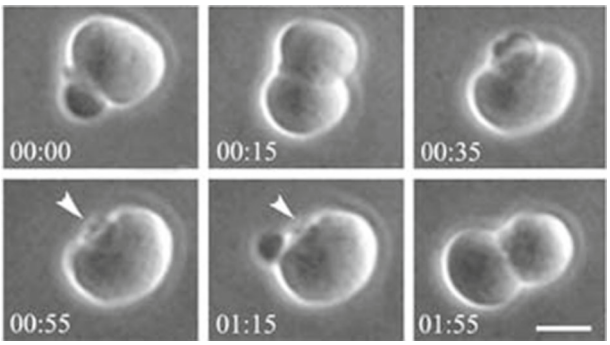

Fig. 1 Cell oscillation experiment from time 00:00 to 00:55, a ring moves from one end to the other end. Starting from 01:15, the ring moves back (from Paluch et al. 2005, scale bar, 5 μm.)

1 Introduction

Cell division and migration are two of the most important functions of living cells. Cell division and migration require shape changes in which actin polymerization and myosin motors play a central role. During the cytokinesis, an actomyosin cortex underneath the membranes generates contractile forces (Zhang and Robinson 2005). The constriction of an actomyosin ring at the cell equator results in the cytokinetic furrow (Cabernard et al. 2010). Due to the contractility force of the actin filaments exert to the membrane, the inside of the cell may maintain a high hydrostatic pressure (Charras et al. 2008). In the case of breakage of the actin cortex, which results in a local disconnection from the membrane, the high pressure drives the membrane bulge outward, which is called cell blebbing (Charras and Paluch 2008). Cell blebbing can release the polar pressure and stabilize the process of cytokinesis. The polarized pressure could be due to spatial localization of myosin, actin, or actin-binding proteins. However, during some conditions there is a large imbalance of the contraction force between the actomyosin cortex and the breakage, the cortex turnover can not stabilize the cytokinesis and it will develop the cell oscillations, and thus a failure of the cytokinesis (Sedzinski et al. 2011).

There are some experiments and mathematical modeling that have been done in the study of cell oscillations. Recently, an experiment (Paluch et al. 2005) comes to our attention in which the authors found an interesting cell oscillation (Fig. 1) which gives us a chance to examine carefully the mechanism based on actomyosin dynamics, and it may be used for explaining the cell polarization in cell division and migration. In the experiment, a constriction ring once formed moves from one end of the cell to the other end, and then moves back across the cell. Such back and forth movement repeats and results in the oscillation of the cell membrane.

In Sedzinski et al. (2011), the authors did further experiments and mathematical modeling about the oscillations. They examined the conditions that could result in the cell oscillations. The cell oscillations are mostly due to the competition between cortex turnover and contraction dynamics. They found that the polar bleb formation

may release the tension of the cortex and help for successful cytokinesis. A faster cortex turnover than the contraction dynamics will most likely to drive a cell oscillation.

In this paper, we propose a mathematical tool, which is called diffusive modeling, to do the computational modeling of cell membrane shape transformation. In this modeling, we considered the following facts that could contribute to the cell oscillations: membrane elastic bending energy, actomyosin dynamics, line tension of the cortex ring, osmotic pressure, and membrane lipid flow. Membrane lipid flow, sometimes being ignored in some models, is considered to be a very important part in our modeling. The surface cortex breakage is due to a large pressure jump of the pressure from the inside to the outside of the cell. This jump is mostly contributed by osmotic pressure. Water permeating into the cell generates the osmotic pressure. It is resisted by the membrane surface tension. A surface breakage may occur when the surface tension is bigger than a threshold value. After a surface breakage, the lipids will be driven to flow from the actomyosin cortex to the bulging part. During the process, lipid transferring is competing with actomyosin turnover. A success oscillation requires a relatively faster lipid flowing speed. However, in our modeling, we do not consider the polar blebs, like that in Sedzinski et al. (2011).

Our purpose is to develop a phase-field model to compare simulation cell shapes to phase contrast images of cell fragments. Here, we focus on the comparison of the cell shape qualitatively to microscopy images. Ultimately, we can compare gradients of actin or myosin (or other proteins) from a spatial model to fluorescent protein tags from experiments. We start from the experiments and setting from Paluch et al. (2005). Figure 2 shows a period of the oscillation. The non-uniform cortex stress results in the breakage of the actomyosin cortex (Gucht et al. 2005), and forms a hole in the cortex. After an initial rapture of the actin gel, the cell membrane is divided into two components, Γ_1 with actin gel and Γ_2 initially devoid of actin and myosin. Due to the actin polymerization and depolymerization, gradually actin will be recruited to the surface Γ_2. Myosin II is attaching to the actin filaments and sliding to exert the stress force. It can also detach from actin filaments to the cytosol by the depolymerization of actin filaments. On the other hand, it can attach to the actin filaments at any position. A set of formulae is used to describe the dynamics of actin and myosin II and calculate their concentrations on different components. Because the concentrations of myosin II at different components are changing in time, the surface tension, which is proportional to the density of the myosin II motors, is also changing in time. The different values of surface tension at different parts of the cell membrane finally drive the lipid molecules from one component to the other, and change the area of Γ_1 and Γ_2. This gives an explanation of the cell oscillations.

As we mentioned before, to further determine the shape of the cell during the oscillation, we also need to consider some other facts, such as the line tension between the two components of a collating cell, the surface tension, the elasticity of the lipid membrane, osmotic pressure, and membrane lipid flow. We will examine those facts in details and propose a system including the transformation of the cell membrane and the dynamics of the actin and myosin inside the cell.

Numerically, one classical method for simulating an evolving interface is to employ a mesh that has grid points on the interfaces, and deforms according to the motion of the boundary, such as the boundary integral and boundary element methods (cf.

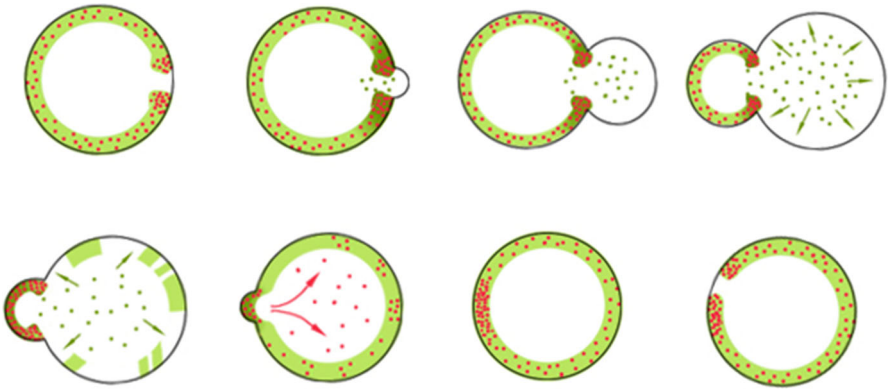

Fig. 2 A period of the cell oscillation (actin gel is colored in green; and the red dots represent the myosin II) (Color figure online)

Cristini et al. 1998; Toose et al. 1995; Khayat 1991 and their references). Keeping track of the moving mesh may entail computational difficulties and large displacement in internal domains may cause mesh entanglement. Typically, sophisticated remeshing schemes have to be used in these cases. We turned to the energetic phase-field models that offer many advantages including the easy treatment of topological changes of the interface (Lowengrub and Truskinovsky 1998), similar to the popular level set formulations (Osher and Fedkiw 2002; Chang et al. 1996). In Zhuan and Kunkun (2013), one computational model based on the phase-field method is developed to describe the a complicated biological process which couples the cell movement and cell morphogenesis with the dynamic behaviors of actin assemble into actin filaments, the physiological functions of myosin, and the interaction between the cell and the substrate. Up to now, we already published a serial of our works in this field, including the phase-field model and its theoretical analysis (Du et al. 2005a; Rui et al. 2016), simulations for equilibrium vesicle shapes (Du et al. 2004, 2005b, 2006), vesicle transformations in fluid fields (Du et al. 2009) and retrieval of topological information within our phase-field framework (Du et al. 2005c).

Following the approach of the phase-field formulations for multi component vesicles studied in Wang and Du (2008), in this paper, we formulate the mathematical model within a phase-field framework. Due to the complexity of the system, we compared our numerical results with those find in biological experiments (Gucht et al. 2005).

The paper is organized as follows: in Sect. 2, we present the mathematical model for the cell oscillations, including the actomyosin dynamics, the energy formulations, membrane lipid dynamics, and osmotic flows. In Sect. 3, we present the phase-field formulations associated with the mathematical model. In Sect. 4, we discuss the discretization schemes and some detailed implementation issues. Spectral methods are used the same as that in Du et al. (2006) due to their high accuracy in calculating the derivatives in space. In Sect. 5, we assemble some interesting experiments of the oscillations triggered by some artificial breakages. We also simply explain the effects of changes in different parameters. Those simulations are compared with biological

findings. We then make some concluding remarks and present the direction of our future work in Sect. 6.

2 Mathematical Model for Cell Oscillations

In this section, we first propose a mathematical model to explain the oscillations. This model includes the actomyosin dynamics, energy formulations, and membrane lipid dynamics. In Sect. 3, we derive the detail phase-field formulations of the mathematical model for numerical simulations.

2.1 Actomyosin Dynamics

The oscillation always starts from a breakage of the underlying actin gel (Paluch et al. 2005; Gucht et al. 2005). The breakage is believed due to the uneven distribution of the actin gel. In the beginning, the actin cortex is only locally ruptured. Around the ruptured hole, a constriction ring forms. This ring divides the cell membrane into two components. One component is devoid of actin in the beginning and bulges out. As time goes on, actin monomers polymerize onto that component gradually. The other component inherits the original actin cortex. Due to the different concentration of the actin and myosin II, the two components have totally different behavior, as one bulges out and grows, while the other component shrinks. Denote the two components by Γ_1 and Γ_2. we have $|\Gamma_1 \cap \Gamma_2| = 0$, $\partial\Gamma_1 \cap \partial\Gamma_2 = \gamma$, and $\Gamma_1 \cup \Gamma_2 = \Gamma$. The ring γ is in between two components and Γ is the whole membrane. During the oscillation process, the area of the two components $|\Gamma_1|$ and $|\Gamma_1|$ are changing. One is expanding, while the other is shrinking. The lipids may move from one component to the other. But the total number of the lipid molecules are fixed. It is known that the lipid membrane can sustain a maximal area expansion of around 2–5% (Boal 2002). Suppose the nature surface area is s. We can make a constraint of the total surface area as

$$|\Gamma_1| + |\Gamma_2| = s. \tag{1}$$

Note that in our final energy formulation (26), this area constrain is penalized to the total energy which actually allows a small area expansion.

Denote the concentrations of the actin on Γ_1 as m_1, on Γ_2 as m_2. Also, we denote the concentrations of the myosin II on Γ_1 as y_1, on Γ_2 as y_2. Here we assume the concentrations of actin and myosin II are uniform on each component for simplicity. The non-uniform concentration is much more common, and some studies are given in Hu et al. (2006). We have different density values of the actin monomers m_0 and myosin II s_0 within the cell. Because of the conservation of the mass, we have the following equations

$$m_0 \mathrm{Vol}(\Gamma) + m_1|\Gamma_1| + m_2|\Gamma_2| = C_m, \tag{2}$$

$$y_0 \mathrm{Vol}(\Gamma) + y_1|\Gamma_1| + y_2|\Gamma_2| = C_y \tag{3}$$

where C_m and C_y are the total mass of actin and myosin II.

Now, we can consider the growth of the actin gel beneath the membrane. It is known that the polymerization occurs at the *plus* end of the actin filaments attached to the membrane, whereas the depolymerization occurs at the other *minus* end (Sekimoto et al. 2004; Noireaux et al. 2000). Thus, the growth velocity of the actin gel can be formulated by

$$\frac{\mathrm{d}m_i}{\mathrm{d}t} = k_{\mathrm{on}} m_0 - k_{\mathrm{off}} \tag{4}$$

for $i = 1, 2$. The value of k_{on} is suggested at 0.032 s^{-1} and k_{off} is suggested at 2.0 nm s^{-1} (Gucht et al. 2005). The growth of actin filaments here does not take the polarity of the actin filament into the account.

Myosin II attaches on the actin filaments. It disassembles to the cytosol during the depolymerization of actin filaments. On the other hand, it attaches to the filaments at any position.

$$\frac{\mathrm{d}y_i}{\mathrm{d}t} = m_i (k^y_{\mathrm{on}} y_0 - k^y_{\mathrm{off}} y_i) \tag{5}$$

where k^y_{on} is the attaching rate of myosin and k^y_{off} is the detaching rate, y_0, y_1 and y_2 are the concentration of myosin II in cytosol, Γ_1 and Γ_2.

2.2 Energy Formulations

Closed cell membranes or vesicles, in most of the case, are composed by unified lipid bilayer structure. The geometry of vesicles theoretically are determined by minimizing energy with contributions of the bending resistance, which is called elastic bending energy, first studied by Ciarlet (1998), Ciarlet (2000). It is based on the principle that the equilibrium shape of such a membrane is determined by minimizing the elastic bending energy:

$$W = \int_\Gamma a_1 + a_2 (H - c_0)^2 + a_3 G \, \mathrm{d}s, \tag{6}$$

where H is the mean curvature of the membrane surface, a_1 is the surface tension, a_2 the bending rigidity and a_3 the stretching rigidity, c_0 is the spontaneous curvature that describes the asymmetry effect of the membrane or its environment, G is the Gaussian curvature. In general, c_0 is assumed to be constant (Lipowsky 1992) but it can also be variable (Seifert 1993). The last term in (6), which is equal to the Euler–Poincare index, representing the topological structure of the membrane which has also been formulated and studied in the context of the energetic variational formulation (Du et al. 2005c). In the whole process, the cell membrane is a uniform lipid bilayer.

Each component has a different parameter value representing surface tension and bending rigidity. The bending energy is formulated as follows:

$$W = \sum_{i=1}^{2} \int_{\Gamma_i} \left(\alpha_i + \kappa_i (H - c_i)^2 + \kappa_i' G\right) \mathrm{d}S. \tag{7}$$

For simplicity, we take elastic bending modules $\kappa_1 = \kappa_2 = \kappa$ to be constant, spontaneous curvature $c_1 = c_2 = c$ and bending module $\kappa_1' = \kappa_2' = \kappa'$ to be another two constants. However, due to the stress from the actomyosin system, the surface tension depends on the concentrations of myosin and actin. Here, we model it as a linear function of the concentration of myosin II, i.e.,

$$\alpha_i = a_1 y_i + a_0 \tag{8}$$

for $i = 1, 2$. Obviously, a_0 is the default surface tension for the cell membrane devoid actin and myosin.

Besides the bending energy, other facts determine the shape of the cell membrane include the line tension energy and osmotic potential energy. The line tension energy from the ring between the two components can be formulated either $\delta|\gamma|$ or $\frac{1}{2}\delta|\gamma|^2$, the energy of a spring. Osmotic pressure regulates the permeate flow of the membrane, and thus the total volume of the cell (Stewart et al. 2011; Zoniz and Munnik 2007). One compartment bulges out is related to the volume change of the cell. Osmotic pressure is proportional to the salt density difference between the inside and the outside of the cell, i.e., $P = c(\rho_0 - \rho)$, where ρ_0 is the outside salt density and ρ the inside salt density, c is a proportional constant. When $\rho = \rho_0$, inside and outside get balanced. On the other hand, $\rho = m/V$, where m is the mass of inside salt, V is the cell volume. We can calculate the osmotic potential energy by

$$E_{os} = c \int_{V_0}^{V} (\rho_0 - m/V)\mathrm{d}V = -(mc \log(V) - c\rho_0 V) + (mc \log(V_0) - c\rho_0 V_0).$$

Combine constants and take off the potential offset, the osmotic potential energy to be used in our model is as following

$$E_{os} = -\tau_0 \log(\mathrm{Vol}(\Gamma)) + \tau_1 \mathrm{Vol}(\Gamma).$$

where $\tau_0 = mc$ and $\tau_1 = c\rho_0$ are two osmotic coefficients. When $\mathrm{Vol}(\Gamma) = \tau_0/\tau_1$, the osmotic potential arrives minimum, i.e., inside and outside get balanced with same salt density.

Take into account of the elastic bending energy, line tension energy and the osmotic potential, we have the following total energy to describe the shape of the oscillating cell membrane.

$$E = \sum_{i=1}^{2} \int_{\Gamma_i} \alpha_i + \kappa_i (H - c_i)^2 + \kappa_i' G \,\mathrm{d}S + \frac{1}{2}\delta|\gamma|^2 - \tau_0 \log(\mathrm{Vol}(\Gamma)) + \tau_1 \mathrm{Vol}(\Gamma) \tag{9}$$

where the line tension coefficient δ and osmotic pressure coefficient τ are treated as constants. The Gaussian curvature bending rigidity κ_i' values the same for the two parts due to the uniform lipid bilayer. From the classic Gauss–Bonnet formula, the integration of the Gaussian curvature of a closed surface is the Euler number, which is a constant if no topological change. Thus, we can ignore this term as there are no topological changes in the oscillations.

2.3 Cell Membrane Lipid Dynamics

The double-layer lipid membrane exhibit a degree of fluidity (Evans and Skalak 1980). With the surface tension on different components, the lipid molecules can transport between the two components. We know that at any moment, with prescribed surface area $|\Gamma_1| = A_1$ and $|\Gamma_2| = A_2$, the cell shape is always determined by minimizing the total energy (9). We can adapt the penalty methods for this constraint optimization problem. Given a large penalty constant M, the whole system minimizes the following total energy

$$E_M = E + \frac{1}{2}M(|\Gamma_1| - A_1)^2 + \frac{1}{2}M(|\Gamma_2| - A_2)^2 \tag{10}$$

where energy E is defined by (9). This penalty form can be rewritten with the Lagrange multipliers. $\{\Lambda_i = M(|\Gamma_i| - A_i)\}_1^2$ as M large enough. The surface interior stress p_i is proportional to the Lagrange terms, i.e.,

$$p_i \sim \Lambda_i = M(|\Gamma_i| - A_i)$$

for $i = 1, 2$. Due to the difference in the stress in two components, the lipids move from one part to another part. The speed is assumed to be proportional to the stress difference. Therefore, we have

$$\frac{\mathrm{d}A_1}{\mathrm{d}t} = \lambda M[(|\Gamma_1| - A_1) - (|\Gamma_2| - A_2)], \tag{11}$$

$$\frac{\mathrm{d}A_2}{\mathrm{d}t} = -\frac{\mathrm{d}A_1}{\mathrm{d}t} \tag{12}$$

where λ is a constant to describe the lipid motility.

2.4 Osmotic Flow

With the osmotic pressure, the water moves in or out the cell and thus changes the cell volume. However, the water cannot move in and out of the cell completely freely. The movement rate of the water is depending on the water pressure, osmotic pressure and surface area. In our model, the surface area is fixed. The water pressure and osmotic pressure come from the variation of the total energy (9). With the same idea handling the membrane lipid dynamics, we can add a penalty term for the volume, and thus measure the pressure for the osmotic flow. Select a large penalty constant,

for simplicity we still denote it as M, which can be the same value or a different value with the penalty constant for the surface area. The total energy (10) further becomes

$$E_M = E + \frac{1}{2}M(|\Gamma_1| - A_1)^2 + \frac{1}{2}M(|\Gamma_2| - A_2)^2 + \frac{1}{2}M(\mathrm{Vol}(\Gamma) - V)^2. \quad (13)$$

This penalty form is equivalent to those with the Lagrange multipliers. The Lagrange multiplier $\Lambda = M(\mathrm{Vol}(\Gamma) - V)$. All the pressures together including the osmotic pressure and the pressure due to the membrane contractions can be described by the Lagrange multiplier. Therefore, the osmotic flowing rate is proportional to Λ, as the surface area is fixed. We have

$$\frac{\mathrm{d}V}{\mathrm{d}t} = \mu M((\mathrm{Vol}(\Gamma) - V) \quad (14)$$

where μ is a constant to describe the cell membrane permeability. For a system with small μ, the permeate flow is very slow, and thus the cell volume is not easy to change.

2.5 Model Summary

All together, we build a mathematical model for the actomyosin driven cell oscillations: At any time t, finding the shape of Γ_1 and Γ_2 to minimize the total energy (13) with the dynamics of the actomyosin system (4), (5), the dynamics of surface area (11), (12), osmotic flow (14) and the mass conservation (1), (2), (3).

It is not trivial to solve the system described in this mathematical model. The major difficulty is to track the surface shape changes. One can simplify the model by thinking each component of the cell membrane is part of a perfect sphere, but this may not be the case. In particular, here we take into account the elastic bending energy of the lipids. Phase-field method has advantages in tracking the surface evolving under a uniform Cartesian grid. We already built the package in simulating the multi-component vesicles (Wang and Du 2008) in 3D by phase-field method we decide to use phase field method to solve this problem. The detailed formulations are given in the following section.

3 Phase-Field Formulations

We follow our previous approach in the study of multi-component vesicles (Wang and Du 2008), which is summarized as follows. We start by introducing a pair of phase-field functions $(\phi(\mathbf{x}), \eta(\mathbf{x}))$, defined on a physical (computational) domain Ω in the three-dimensional space. The function $\phi = \phi(\mathbf{x})$ is used so that the level set $\{\mathbf{x} : \phi(\mathbf{x}) = 0\}$ determines the membrane Γ, while $\{\mathbf{x} : \phi(\mathbf{x}) > 0\}$ represents the interior of the membrane (denoted by Ω_i) and $\{\mathbf{x} : \phi(\mathbf{x}) < 0\}$ the exterior (denoted by Ω_e). In the phase-field models of a single component vesicle, this is the only phase-field function used (Du et al. 2004).

Next, we take another closed surface $\Gamma_\perp$ defined on the domain Ω and being perpendicular to Γ, such that it is the zero level set $\{\mathbf{x} : \eta(\mathbf{x}) = 0\}$ of a phase-field function

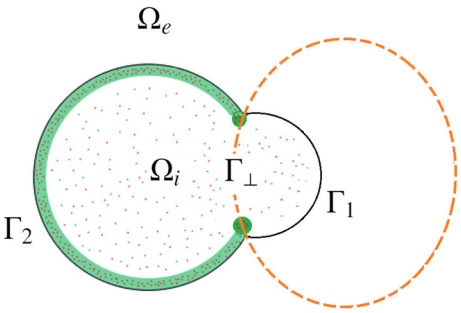

Fig. 3 Membrane $\Gamma = \Gamma_1 \cup \Gamma_2$, is described by phase file function $\phi(\mathbf{x})$. The label surface $\Gamma_\perp$, defined by phase-field function $\eta(\mathbf{x})$, cuts the surface Γ into two components Γ_1 and Γ_2 (Color figure online)

$\eta = \eta(x)$ in Ω with $\{\mathbf{x} : \eta(\mathbf{x}) > 0\}$ being the interior of $\Gamma_\perp$ and $\{\mathbf{x} : \phi(\mathbf{x}) < 0\}$ the exterior. We thus take the part of Γ in the interior of $\Gamma_\perp$ as the first component Γ_1 and the remain part of Γ makes up the second component Γ_2. Note that there may be many choices to select $\Gamma_\perp$, but we are mostly interested in the level set $\{\mathbf{x} : \eta(\mathbf{x}) = \phi(\mathbf{x}) = 0\}$ which gives the ring between the two components of the vesicle, with $\{\mathbf{x} : \eta(\mathbf{x}) > 0$ and $\phi(\mathbf{x}) = 0\}$ representing one component of the membrane, while $\{\mathbf{x} : \eta(\mathbf{x}) < 0$ and $\phi(\mathbf{x}) = 0\}$ the other component (Fig. 3).

In the phase-field model, the functions η and ϕ are forced to be nearly constant-valued except in thin transition layers the surfaces Γ and $\Gamma_\perp$, respectively. We use two small positive constant parameters ϵ and ξ to characterize the widths of the thin layers (also called the diffuse interfaces).

Similar to Wang and Du (2008), we have the phase-field formulation for the surface energy defined by

$$E_{\text{surf}}(\phi, \eta) = \frac{3\sqrt{2}}{4} \int_\Omega \alpha(\eta) \left(\frac{\epsilon}{2} |\nabla \phi|^2 + \frac{1}{4\epsilon} (\phi^2 - 1)^2 \right) \mathrm{d}x \tag{15}$$

where the variable surface tension is given by

$$\begin{aligned} \alpha(\eta) &= \frac{1}{2}(\alpha_1 + \alpha_2 + (\alpha_1 - \alpha_2) \tanh(\eta/\epsilon)) \\ &= a_0 + \frac{a_1}{2}(y_1 + y_2 + (y_1 - y_2) \tanh(\eta/\epsilon)) \end{aligned} \tag{16}$$

so that α_1 is the value of surface tension of one component and α_2 is the other. As revealed in Wang and Du (2008), we can always assume $\phi(\mathbf{x}) \sim \tanh(d(\mathbf{x}, \Gamma)/(\sqrt{2}\epsilon))$ and $\eta(\mathbf{x}) \sim \tanh(d(\mathbf{x}, \Gamma_\perp)/(\sqrt{2}\xi))$ for the phase-field functions. With this ansatz, we can check that as ϵ and ξ tend to 0, that is, in the sharp interface limit,

$$E_{\text{surf}}(\phi, \eta) \to \sum_i \int_{\Gamma_i} \alpha_i \, \mathrm{d}S \, .$$

Similarly, we have the following phase-field formulations

$$\frac{3\sqrt{2}}{4}\int_\Omega \left(\frac{\epsilon}{2}|\nabla\phi|^2+\frac{1}{4\epsilon}(\phi^2-1)^2\right)\mathrm{d}x \to |\Gamma|, \tag{17}$$

$$S_1(\phi,\eta)=\frac{3\sqrt{2}}{4}\int_\Omega \frac{1+\tanh(\eta/\xi)}{2}\left(\frac{\epsilon}{2}|\nabla\phi|^2+\frac{1}{4\epsilon}(\phi^2-1)^2\right)\mathrm{d}x \to |\Gamma_1| \tag{18}$$

and

$$S_2(\phi,\eta)=\frac{3\sqrt{2}}{4}\int_\Omega \frac{1-\tanh(\eta/\xi)}{2}\left(\frac{\epsilon}{2}|\nabla\phi|^2+\frac{1}{4\epsilon}(\phi^2-1)^2\right)\mathrm{d}x \to |\Gamma_2|, \tag{19}$$

$$E_{\text{elastic}}(\phi,\eta)=\frac{3\sqrt{2}}{8}\int_\Omega \frac{\kappa}{2\epsilon}\left(\epsilon\Delta\phi+(\frac{1}{\epsilon}\phi+c\sqrt{2})(1-\phi^2)\right)^2\mathrm{d}x \to \int_\Gamma \kappa(H-c)^2\,\mathrm{d}S. \tag{20}$$

In above convergence formula, one can think that our phase-field formulation at the left-hand side is an approximation of the data at the right hand side of the convergence arrow. But if we choose ϵ and ξ smaller enough, the approximation error can be ignored.

The length of the ring between two components is approximated by functional

$$L(\phi,\eta)=\frac{9}{8}\int_\Omega\left[\frac{\epsilon}{2}|\nabla\eta|^2+\frac{1}{4\epsilon}(\eta^2-1)^2\right]\left[\frac{\epsilon}{2}|\nabla\phi|^2+\frac{1}{4\epsilon}(\phi^2-1)^2\right]\mathrm{d}x \tag{21}$$

and the volume inside Γ is formulated by

$$V(\phi)=\frac{1}{2}\int_\Omega 1+\phi\,\mathrm{d}x. \tag{22}$$

Thus, the total energy in the phase-field framework is

$$\begin{aligned}E_M(\phi,\eta)=&E_{\text{surf}}(\phi,\eta)+E_{\text{elastic}}(\phi,\eta)+\frac{1}{2}\delta L^2(\phi,\eta)-\tau_0\log(\mathrm{V}(\phi))\\&+\tau_1\mathrm{V}(\phi)+\frac{M}{2}(S_1(\phi,\eta)-A_1)^2+\frac{M}{2}(S_2(\phi,\eta)-A_2)^2\\&+\frac{M}{2}(\mathrm{V}(\phi)-V)^2.\end{aligned} \tag{23}$$

Following the approach in Wang and Du (2008), to maintain the consistency of the phase-field model which is based on ϕ and η having the tanh profiles and the orthogonality between Γ and $\Gamma_\perp$, additional constraints are imposed. First of all, the orthogonality constraint on the normal directions of the two surfaces, written in our phase-field formulations, can be enforced by $\nabla\phi\cdot\nabla\eta=0$ on or near the phase boundary $\{\mathbf{x}:\phi(\mathbf{x})=\eta(\mathbf{x})=0\}$. This orthogonality constraint can be enforced everywhere by penalizing

$$P(\phi,\eta)=\int_\Omega\frac{\epsilon}{2}|\nabla\phi\cdot\nabla\eta|^2\,\mathrm{d}x\ . \tag{24}$$

Secondly, to better maintain the tanh profile of η, especially for the case of a large line tension energy, we have two options, one is to add a small regularization term, much like the bending elastic energy for ϕ but with a very small bending rigidity; another option is to regularize through the following functional

$$Q(\eta) = \int_\Omega \left(\frac{\xi}{2}|\nabla\eta|^2 - \frac{1}{4\xi}(\eta^2-1)^2\right)^2 \mathrm{d}x\ , \tag{25}$$

which also vanishes for any function η having a tanh profile.

We can also convert these constraints into a penalty formulation with another large penalty constant N. Thus, we will minimize the energy

$$\begin{aligned}\mathcal{E}_M(\phi,\eta) = {} & E_{\text{surf}}(\phi,\eta) + E_{\text{elastic}}(\phi,\eta) + \frac{1}{2}\delta L^2(\phi,\eta) - \tau_0\log(\mathrm{V}(\phi)) \\ & + \tau_1\mathrm{V}(\phi) + \frac{M}{2}(S_1(\phi,\eta)-A_1)^2 + \frac{M}{2}(S_2(\phi,\eta)-A_2)^2 \\ & + \frac{M}{2}(\mathrm{V}(\phi)-V)^2 + \frac{N}{2}(P(\phi,\eta))^2 + \frac{N}{2}(Q(\eta))^2.\end{aligned} \tag{26}$$

To search for the energy minimizers, we adopt a gradient flow approach which has been very effective for solving the phase-field model of single- or multi-component vesicles (Du et al. 2004, 2006; Wang and Du 2008). The equations for the gradient flow are given by:

$$\phi_t = -r\frac{\delta\mathcal{E}_M}{\delta\phi}, \quad \eta_t = -r\frac{\delta\mathcal{E}_M}{\delta\eta} \tag{27}$$

where coefficient r is a time scale, representing the membrane shape changing speed. The variation of $\frac{\delta\mathcal{E}_M}{\delta\phi}$, and $\frac{\delta\mathcal{E}_M}{\delta\eta}$ can be calculated by the summation of the variation of each term. Those calculations can be found in Du et al. (2009), Wang and Du (2008). For simplicity, here we list some of them here

$$\frac{\delta E_{\text{surf}}(\phi,\eta)}{\delta\phi} = \frac{3\sqrt{2}}{4}\alpha(\eta)\left(\epsilon\Delta\phi + \frac{1}{\phi}(\phi^3-\phi)\right) \tag{28}$$

$$\frac{\delta E_{\text{surf}}(\phi,\eta)}{\delta\eta} = \frac{3\sqrt{2}}{4}\alpha'(\eta)\left(\frac{\epsilon}{2}|\nabla\phi|^2 + \frac{1}{4\epsilon}(\phi^2-1)^2\right) \tag{29}$$

The whole system used to describe the oscillation is (27) with the dynamics of the actomyosin system (4), (5), the dynamics of surface area (11), (12), and the mass conservation (1), (2), (3). The model equations are summarized below.

$$
\begin{aligned}
&\phi_t = -r\frac{\delta \mathcal{E}_M}{\delta \phi};\\
&\eta_t = -r\frac{\delta \mathcal{E}_M}{\delta \eta};\\
&\frac{\mathrm{d}m_i}{\mathrm{d}t} = k_{\mathrm{on}} m_0 - k_{\mathrm{off}} \quad \text{for} \quad i = 1, 2;\\
&\frac{\mathrm{d}y_i}{\mathrm{d}t} = m_i (k^y_{\mathrm{on}} y_0 - k^y_{\mathrm{off}} y_i) \quad \text{for} \quad i = 1, 2;\\
&\frac{\mathrm{d}A_1}{\mathrm{d}t} = \lambda M[(S_1(\phi, \eta) - A_1) - (S_2(\phi, \eta) - A_2)];\\
&\frac{\mathrm{d}A_2}{\mathrm{d}t} = -\frac{\mathrm{d}A_1}{\mathrm{d}t};\\
&\frac{\mathrm{d}V}{\mathrm{d}t} = \mu M(\mathrm{V}(\phi) - V);\\
&m_0 V(\phi) + m_1 A_1 + m_2 A_2 = C_m;\\
&y_0 V(\phi) + y_1 A_1 + y_2 A_2 = C_y
\end{aligned}
\tag{30}
$$

with initial values at time $t = 0$

$$\phi(0) = \phi_0, \quad \eta(0) = \eta_0, \quad A_1(0) = S_1(\phi_0, \eta_0), \quad A_2(0) = S_2(\phi_0, \eta_0),$$

and $m_1(0), m_2(0), y_1(0), y_2(0)$. Also the prescribed constants including

$$r, \lambda, \mu, k_{\mathrm{on}}, k_{\mathrm{off}}, C_m, C_y, a_0, a_1, c, \kappa, \delta, \tau_0, \tau_1, M, N, \epsilon, \xi.$$

Note that a_0, the intrinsic surface tension of the cell membrane without actin and myosin is negligible. Because the total surface area is fixed, the surface tension contribution from a_0 to the total energy keeps to be constant. So in all of our experiments, we just set $a_0 = 0$.

4 Numerical Schemes

For spatial discretization, we use Fourier spectral methods on a regular 3D Cartesian grid. Due to the regularization effect of the finite transition layer, for fixed ϵ, ξ, the solutions exhibit high-order regularities and thus making spectral methods very efficient with the help of FFT routines.

There are a number of options for the time discretization. For simplicity, we discretize the system of equations from (30) in time using forward Euler's method as follows: (30):

$$\frac{\phi^{n+1} - \phi^n}{\Delta t} = -r\frac{\delta \mathcal{E}_M}{\delta \phi}(\phi^n, \eta^n); \tag{31}$$

$$\frac{\eta^{n+1} - \eta^n}{\Delta t} = -r\frac{\delta \mathcal{E}_M}{\delta \eta}(\phi^n, \eta^n); \tag{32}$$

$$\frac{A_1^{n+1}-A_1^n}{\Delta t}=\lambda M[(S_1(\phi^{n+1},\eta^{n+1})-A_1^n)-(S_2(\phi^{n+1},\eta^{n+1})-A_2^n)]; \quad (33)$$

$$\frac{A_2^{n+1}-A_2^n}{\Delta t}=-\frac{A_1^{n+1}-A_1^n}{\Delta t}; \quad (34)$$

$$\frac{V^{n+1}-V^n}{\Delta t}=\mu M(V(\phi^{n+1})-V^n); \quad (35)$$

$$\frac{m_i^{n+1}-m_i^n}{\Delta t}=k_{\text{on}}m_0^n-k_{\text{off}} \quad \text{for} \quad i=1,2; \quad (36)$$

$$\frac{y_i^{n+1}-y_i^n}{\Delta t}=m_i^n k_{\text{on}}^y y_0^n-k_{\text{off}}y_i^n \quad \text{for} \quad i=1,2; \quad (37)$$

$$m_0^{n+1}=(C_m-m_1^{n+1}A_1^{n+1}-m_2^{n+1}A_2^{n+1})/V(\phi^{n+1}); \quad (38)$$

$$y_0^{n+1}=(C_y-y_1^{n+1}A_1^{n+1}-y_2^{n+1}A_2^{n+1})/V(\phi^{n+1}). \quad (39)$$

The whole system is split into three parts. Equations (31)–(32) solve the phase-field dynamics, or the shape of the cell with two components. Equations (33)–(35) solve the lipid transferring and osmotic fluid. Equations (36)–(39) solve the actomyosin dynamics.

For the first part, a sufficiently small time step size Δt should be chosen to satisfy the decay of energy, i.e.,

$$\mathcal{E}_M(\phi^{n+1},\eta^{n+1})<\mathcal{E}_M(\phi^n,\eta^n). \quad (40)$$

Note that two different time steps can be used, Δt_1 in Eqs. (31)–(32), and Δt_2 in Eqs. (33)–(39). Latter time step Δt_2 is k times of Δt_1, the time step of former. In another words, we can go k steps Eqs. (31)–(32) with step size $\Delta t_1=\Delta t_2/k$ and then go one step Eqs. (33)–(39) with step size Δt_2. Δt_2 can be fixed to be relatively large, k is always adjusted to be sufficiently large to get a smaller Δt_1 such that the energy decays (40) for every iteration of Eqs. (31)–(32). If a particular time step size violates the energy decreasing principle, we just simply double k and repeat the iterations. It is assured that sufficiently small steps would decrease the energy if the solution is not at a local minimum of the energy, which is always true for our problem. Practically, we will try to half k after some period to increase Δt_1 so that to speed up the iterations. We like to point out that for the most part of in our numerical experiments, although fully adjustable, the step size Δt_1 is kept to be in the interval from 10^{-6} to 10^{-7} and Δt_2 is kept to be 10^{-4}.

There have been some stabilized numerical methods could be used for this type of phase-field equations, such as stabilized semi-implicit Euler methods (Du et al. 2018), exponential time differencing methods (Wang et al. 2016). We believe that those methods could further improve the simulation in terms of efficiency and discrete energy stability. Although we did not try those methods here, in Rui et al. (2014), Rui et al. (2016), we tried the nonlinear CG methods and lowered the cost in finding the energy minimizers.

For this specific problem, one can simplify the problem from 3D to 1D due to the axissymmetric property of the case. Because we already have the full three-

dimensional code package, and for the possible future non-axissymmetric case, we did the fully 3D simulations of this problem. To make our three-dimensional simulations efficient on today's high-performance computing platform, parallel implementation is a useful approach that can be realized on both distributed memory systems via MPI and shared memory systems via OpenMP. As we have done in Wang and Du (2008), in our numerical experiments, we have mostly utilized the OPENMP platform on a shared memory system with 16 CPU cores. One can refer Wang and Du (2008) for detail discussions. We also use the FFTW freeware package which provides necessary interfaces for the parallel implementation of FFT via MPI and OpenMP. Our parallel code is only implemented using the serial interface of FFTW for one-dimensional and two-dimensional discrete FFTs. The scalable performance of our numerical implementation is clearly observed. This provides efficient means for us to conduct extensive three dimensional simulations.

5 Numerical Simulation

In this section, we present the results of the three-dimensional simulations. Throughout this section, we take the domain as the box $[-\pi, \pi]^3$ except otherwise indicated. The domain is divided into 48^3 or 64^3 uniform mesh grids. Also, we choose the phase transition parameters $\epsilon = \xi = 1.25h$.

5.1 Initial Shape and Initial Breakage

For a complete actin cortex without breakage, our mathematical model becomes an energy minimizing process. There is only one component. Because there is no lipid transferring, the cell membrane surface area is fixed. The surface tension energy will be dropped off the total energy. Gradually, the actin and myosin dynamics will reach an equilibrium state. For the actin, the depolymerization rate k_{off} is the same as the polymerization rate of $k_{\text{off}} m_0$. Osmotic pressure is balanced by the surface tension and bending rigidity. The whole system degenerates into the regular one component problem to find surface Γ minimizing the energy

$$E = \int_\Gamma \kappa (H - c)^2 \, \mathrm{d}S - \tau_0 \log(\mathrm{V}(\phi)) + \tau_1 \mathrm{V}(\phi) \tag{41}$$

with fixed surface area $|\Gamma|$. If the actomyosin dynamics do not change the bending rigidity κ and the spontaneous curvature c, the problem degenerates into a static optimization problem, which was already studied in details on paper (Du et al. 2004, 2005b). If the inside salt density is larger than that outside and the osmotic potential by far outpaces the elastic bending energy, water will move inside and force the cell to be spherical. Given a surface area, if the inside salt density is larger than that of the outside, water will permeate into the cell and make it spherical. Also because the sphere always has the smallest elastic bending energy $\int_\Gamma \kappa H^2 \, \mathrm{d}S$, a spherical cell shape is the most often case to be observed.

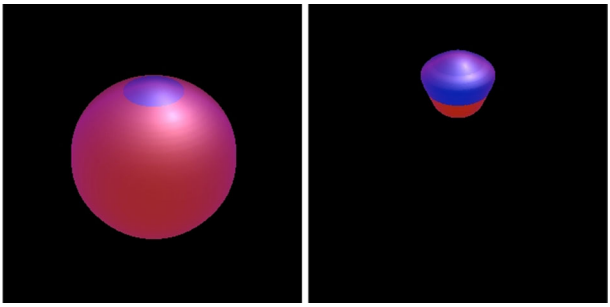

Fig. 4 Initial spherical cell with initial breakage after several runs. Left: the cell surface (0-level set of ϕ), blue colored part is the breakage; right: the ghost surface (0-level set of η) to cut the cell into two components. Both the cell surface and the ghost surface evolve in time. Please refer Wang and Du (2008) for more details (Color figure online)

Fig. 5 One period of the oscillation of cell. From left to right, cut view at time $t = 0.3, 1.0, 2.0, 3.0, 4.0$ (Color figure online)

In the numerical simulation, we can start from an initial shape with initial breakage. In most of the case, the initial shape is a sphere. The initial breakage is artificial. The spherical cell is the zero level set of the first phase-field function ϕ. We construct another phase-field function η whose zero level set cut the sphere a small surface. We can set the ghost surface as a small perfect sphere. Once the initial breakage formed, the initial balance is broken and the cell starts its shape evolution. Figure 4 shows a sphere with initial breakage. Different color describes different components. The blue color in the left image is the breakage. The right picture is the ghost surface, i.e., the zero level set of phase-field function η used to label the breakage.

5.2 Simulations with Artificial Breakages

Figure 5 shows one period of the oscillation of the cell. We use the cut view to see the two components more clearly. Note that the color in the picture represents the density of the myosin II. From blue to red, the myosin II density is from low to high. Pure blue indicate a value of 0, and pure red indicate a value around 2.0. In the beginning, the breakage is void of the myosin II. With time going on, the breakage bulges and grows larger and larger, finally take control of the while surface. The density of myosin II grows significantly as the color goes from blue to red.

This experiment was performed on a 64^3 grid mesh. The parameters we used are as following: time scale $r = \lambda = 1$; linear coefficient for the surface tension $a_1 = 30$, $a_0 = 0$; elastic bending rigidity $\kappa = 1.0$; spontaneous curvature $c = 0$; line tension

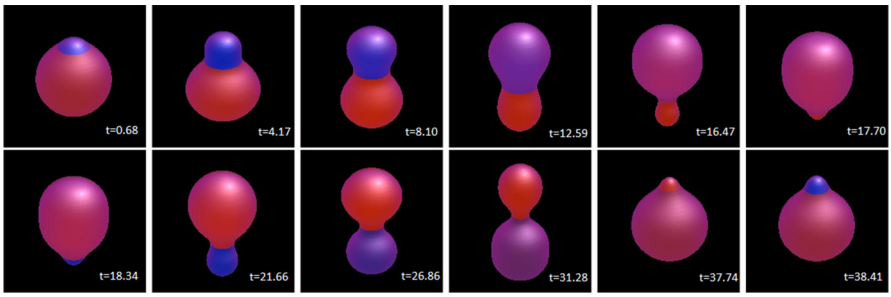

Fig. 6 Oscillation of the cell with artificial breakages. From left to right, first row to the second row, cell images time $t = 0.68, 4.17, 8.10, 12.59, 16.47, 17.70, 18.34, 21.66, 26.86, 31.28, 37.74, 38.41$ (Color figure online)

coefficient $\delta = 1.3$; osmotic pressure coefficients $\tau_0 = 70$, $\tau_1 = 0$; osmotic motility $\mu = 10$; total surface area is 31.14; penalty coefficients $M = N = 10000$. Initial actin distributions $m_0 = 0$, $m_1 = 0.9$, $m_2 = 0$; and myosin II distributions $y_0 = 0$, $y_1 = 0.81$, $y_2 = 0$; actomyosin dynamics coefficients $k_{\text{on}} = 0.5$, $k_{\text{on}}^y = 1.0$, $k_{\text{off}} = k_{\text{off}}^y = 0$.

By dimensional analysis, we can give the units of those quantities. The domain range of x is $[-\pi, \pi]$, in unit μm. The time is in unit second. Bending rigidity κ is in unit $10^{-18} J$. The line tension (Hookean) coefficient δ is in the unit $10^{-12}\text{N}\,\mu\text{m}^{-1}$. Osmotic pressure coefficients τ is in the unit 10^{-18} J. Actomyosin dynamics coefficients k_{on} is in unit 10^{-3} s^{-1}, k_{off} is in unit nm s^{-1}. Actin-myosin distribution m_1, m_2, y_1, y_2 have unit nm, and m_0, y_0 has unit 10^{-3}.

Note that in Fig. 5, the lower component finally disappeared. The oscillation stops. In the biological experiments, after a very short time, another oscillation period starts. To simulate the whole oscillation process, only with the initial breakage is not enough. In our numerical simulation, we periodically set the artificial breakages. For example, we reset the actin and myosin density to zero once the surface area of that component shrinks under 5% of the whole area. Meanwhile, we increase the actin and myosin densities m_0 and y_0 so that the mass is conserved. Just as shown in Fig. 6, the cell periodically oscillates.

The first row of Fig. 6 shows one period. The ring moves from top to bottom, myosin II recruited to the membrane gradually. During the time between 17.70 and 18.34, the lower component shrinks the surface area smaller enough and then we manually reset the actin and myosin densities to 0 to simulate another breakage. This results in the second round of oscillation, with the ring moves from bottom to top. Actin and myosin recruit to the cortex gradually as well. Between the time 37.74 and 38.41, we get another reset of the actin and myosin densities to 0. The third oscillation period begins.

Figure 7 shows the concentration of actin and myosin II during the first two oscillation periods of this simulation. At the time 0, we see the breakage (part II, i.e. Γ_2) is devoid of actin and myosin. As time goes on, Fig. 8 shows that the surface area of part I shrinks and due to the polymerization, the concentrations on both parts grow. At the time about 18, part I gets reset to 0 density of actin and myosin II. With this

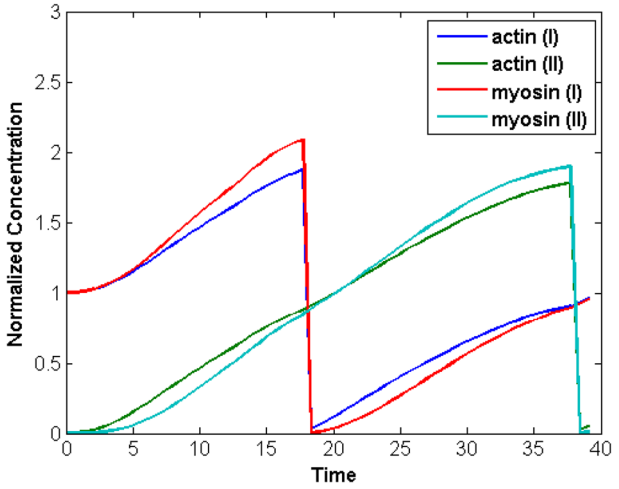

Fig. 7 Plot of the concentration of actin and myosin II during two oscillation periods (Color figure online)

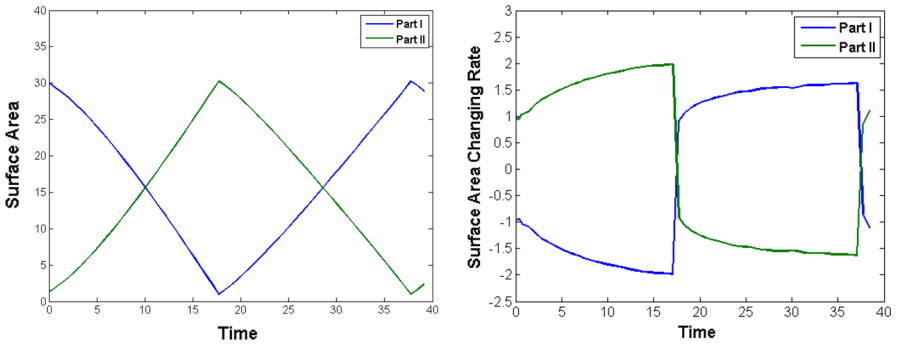

Fig. 8 Plot of the surface area (left) and the surface area changing rate/lipid transferring rate (right) of different parts during two oscillation periods (Color figure online)

artificial breakage, the second period starts. This process can repeat once again and again, resulting in the cell oscillations.

The right plot of Fig. 8 shows the lipid transferring rate (from Eqs. 11, 12) in time. The transferring rate keeps slightly increasing during each oscillation period.

This experiment performed on a 48^3 grid mesh. The parameters we used are as following: time scale $r = \lambda = 1$; linear coefficient for the surface tension $a_1 = 30$, $a_0 = 0$; elastic bending rigidity $\kappa = 1.0$; spontaneous curvature $c = 0$; line tension coefficient $\delta = 1.5$; osmotic pressure coefficients $\tau_0 = 70$, $\tau_1 = 0$; osmotic motility $\mu = 10$; total surface area is 31.24; penalty coefficients $M = N = 10{,}000$. Because we use the penalty method in our formulation, the penalty coefficients should be chosen sufficiently large. Initial actin distributions $m_0 = 1.0$, $m_1 = 1.0$, $m_2 = 0$; and myosin II distributions $y_0 = 1.0$, $y_1 = 1.0$, $y_2 = 0$; actomyosin dynamics coefficients $k_{\text{on}} = 0.25$, $k_{\text{on}}^y = 0.25$, $k_{\text{off}} = k_{\text{off}}^y = 0$.

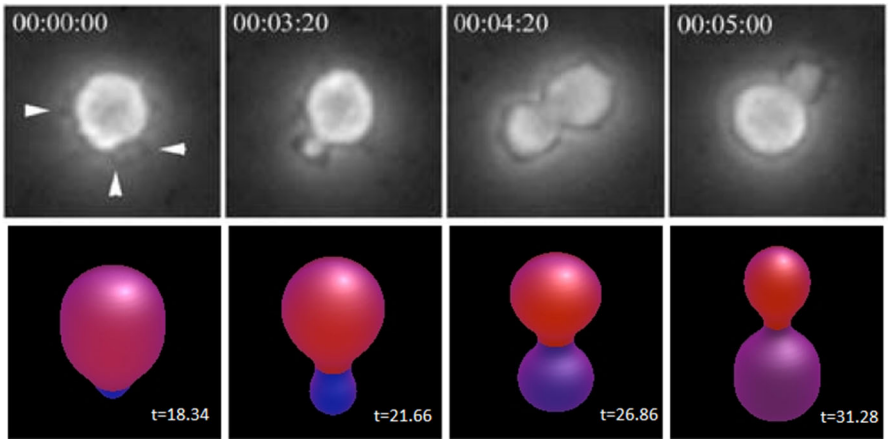

Fig. 9 Comparison of the bio-images with our simulations. First row: the bio-image of cell oscillations from Paluch et al. (2005), bottom: the first four pictures of the second row of Fig. 6 (Color figure online)

Compared with the first simulation, we keep most of the parameters to be the same. One difference is that the actomyosin dynamics coefficients $k_{\text{on}}, k_{\text{on}}^{y}$ are about $1/4$ of the previous one, resulting in slower actomyosin dynamics. One can notice this slow down by comparing the color of the third and fourth pictures between Figs. 5 and 6. Another difference is that we increase the line tension coefficient from 1.3 to 1.5. This change results in a thinner ring in Fig. 6 comparing to that in Fig. 5. For more effects of the parameters for phase-field modeling of the two-component cell membranes, please refer Wang and Du (2008) for more details.

We performed our experiments with different osmotic pressure coefficients. With zero osmotic pressure coefficients, the oscillations still happen. With larger osmotic pressure coefficients ($\tau_0 = 100$), the shape remains spherical with little shrinking. With super large osmotic pressure coefficients ($\tau_0 = 1000$), the shape keeps to be spherical. Although following a man-made breakage, there is still oscillations, we think large osmotic pressure will suppress the breakage and thus lower the oscillation rate as indicated in Paluch et al. (2005).

Figure 9 gives a rough comparison of the bio-images from experiments of L929 fibroblasts (Paluch et al. 2005) with our numerical simulations in our second experiments. The second-row pictures are the same as that of the first four pictures of the second row of Fig. 6. We believe a finer mesh simulation can get better results. For example, one may notice that the cells appear to have regions of higher curvature at the interface of the two compartments when compared to the experimental images.

6 Conclusion

In this paper, we first build a mathematical model to explain the cell oscillations driven by actin and myosin II dynamics. A phase field method is used to solve this problem. Three-dimensional numerical simulations are carried out. With the use of

penalty formulation, our model can effectively calculate the transferring of the lipids from one component to the other. Also because of the penalty formulation, we are able to model the osmotic flow. A simple forward Euler scheme for the numerical implementation is discussed, as well as the possible parallel methods for this problem. In the numerical simulations, we performed artificial breakages which triggers the oscillations. We also compared our numerical results with biological images. The model successfully explained the mechanism based on actomyosin dynamics, and it may be further extended to explain the cell polarization in cell division and migration.

In conclusion, we would like to stress that the current work to be a further step of our previous work for the study of the deformation vesicle membranes. In this work, we begin the consideration of the cell inside structures, including the actin filaments, myosin II and their dynamics. Moreover, a more careful study on the the relation between the parameters in our system and more complex study such as the reaction and diffusion of actin monomers, and interactions of the cell membrane with fluid fields are needed in the future.

Acknowledgements The authors thank the referees for their valuable comments and suggestions. The first author's research is supported by NSF-DMS 1819059 while the second author's research is partially supported by China Fundamental Research of Civil Aircraft under Grant Number MJ-F-2012-04.

References

Boal D (2002) Mechanics of the cell. Cambridge University Press, New York

Cabernard C, Prehoda K, Doe C (2010) A spindle-independent cleavage furrow positioning pathway. Nature 467(7311):91–94

Chang YC, Hou TY, Merriman B, Osher S (1996) A level set formulation of Eulerian interface capturing methods for incompressible fluid flows. J Comput Phys 124:449–464

Charras G, Paluch E (2008) Blebs lead the way: how to migrate without lamellipodia. Nat Rev Mol Cell Biol 9(9):730–736

Charras GT, Coughlin M, Mitchison TJ, Mahadevan L (2008) Life and times of a cellular bleb. Biophys J 94:1836–1853

Ciarlet PG (1998) Introduction to linear shell theory. In: Series in applied mathematics (Paris), vol 1. Gauthier-Villars, Éditions Scientifiques et Médicales Elsevier, Paris

Ciarlet PG (2000) Mathematical elasticity, vol III. In: Studies in mathematics and its applications, vol 29. Theory of shellsNorth-Holland Publishing Co., Amsterdam

Cristini V, Blawzdziewicz J, Loewenberg M (1998) Drop breakup in three-dimensional viscous flows. Phys Fluids 10:1781–1783

Du Q, Liu C, Wang X (2004) A phase field approach in the numerical study of the elastic bending energy for vesicle membranes. J Comput Phys 198:450–468

Du Q, Liu C, Ryham R, Wang X (2005a) A phase field formulation of the Willmore problem. Nonlinearity 18:1249–1267

Du Q, Liu C, Ryham R, Wang X (2005b) Modeling the spontaneous curvature effects in static cell membrane deformations by a phase field formulation. Commun Pure Appl Anal 4:537–548

Du Q, Liu C, Wang X (2005cc) Retrieving topological information for phase field models. SIAM J Appl Math 65:1913–1932

Du Q, Liu C, Wang X (2006) Simulating the deformation of vesicle membranes under elastic bending energy in three dimensions. J Comput Phys 212(2):757–777

Du Q, Liu C, Ryham R, Wang X (2009) Energetic variational approaches in modeling vesicle and fluid interactions. Physica D 238:923–930

Du Q, Ju L, Li X, Qiao Z (2018) Stabilized linear semi-implicit schemes for the nonlocal Cahn-Hilliard equation. J Comput Phys 363:39–54

Evans EA, Skalak R (1980) Mechanics and thermodynamics of biomembranes. CRC Press Inc., Boca Raton
Gucht J, Paluch E, Plastino J, Sykes C (2005) Stress release drives symmetry breaking for actin-based movement. Proc Natl Acad Sci USA 102:7847–7852
Hu J, Matzavinos A, Othmer HG (2006) A theoretical approach to actin filament dynamics. J Stat Phys 128:111–138
Khayat RE (1991) Shape transitions and shape stability of giant phospholipid vesicles in pure water induced by area-to-volume changes. Biophys J 60:825–844
Lipowsky R (1992) Budding of membranes induced by intramembrane domains. J Phys II Fr 2:1825–1840
Lowengrub J, Truskinovsky L (1998) Quasi-incompressible Cahn-Hilliard fluids and topological transitions. R Soc Lond Proc Ser A Math Phys Eng Sci 454:2617–2654
Noireaux V, Goldsteyn RA, Friederich E, Prost J, Antony C, Louvard D, Sykes C (2000) Growing an actin gel on spherical surfaces. Biophys J 278:1643–1654
Osher S, Fedkiw R (2002) The level set method and dynamic implicit surfaces. Springer, Berlin
Paluch E, Piel M, Prost J, Bornens M, Sykes C (2005) Cortical actomyosin breakage triggers shape oscillation in cells and cell fragments. Biophys J 89:724–33
Rui G, Xiaoqiang W, Max G (2014) Simulating vesicle-substrate adhesion using two phase field functions. J Comput Phys 275:626–641
Rui G, Xiaoqiang W, Max G (2016) A two phase field model for tracking vesicle-vesicle adhesion. J Math Biol 73(5):1293–1319
Sedzinski J, Biro M, Oswald A, Tinevez J, Salbreux G, Paluch E (2011) Polar actomyosin contractility destabilizes the position of the cytokinetic furrow. Nature 476(7361):462–466
Seifert U (1993) Curvature-induced lateral phase separation in two-component vesicles. Phys Rev Lett 70:1335–1338
Sekimoto K, Prost J, Jülicher F, Boukellal H, Bernheim-Groswasser A (2004) Role of tensile stress in actin gels and a symmetry-breaking instability. Eur Phys J E 13:247–259
Stewart MP, Helenius J, Toyoda Y, Ramanathan SP, Muller DJ, Hyman AA (2011) Hydrostatic pressure and the actomyosin cortex drive mitotic cell rounding. Nature 469:226–230
Toose EM, Geurts BJ, Kuerten JGM (1995) A boundary integral method for two-dimensional (non)-Newtonian drops in slow viscous flow. J Non-Newton Fluid Mech 60:129–154
Wang X, Du Q (2008) Modelling and simulations of multi-component lipid membranes and open membranes via diffusive interface approaches. J Math Biol 56(3):347–371
Wang X, Ju L, Du Q (2016) Efficient and stable exponential time differencing Runge-Kutta methods for phase field elastic bending energy models. J Comput Phys 316:21–38
Zhang W, Robinson D (2005) Balance of actively generated contractile and resistive forces controls cytokinesis dynamics. Proc Natl Acad Sci 102(20):7186–7191
Zhuan L, Kunkun G (2013) Cell morphodynamics via phase field dynamics model. Acta Chim Sin 71(8):1183–1188
Zoniz L, Munnik T (2007) Life under pressure: hydrostatic pressure in cell growth and function. Trends Plant Sci 12(3):90–97